LASER INTERFEROMETER GRAVITATIONAL WAVE OBSERVATORY

– LIGO –

CALIFORNIA INSTITUTE OF TECHNOLOGY
MASSACHUSETTS INSTITUTE OF TECHNOLOGY

Document Type	**LIGO-T000122-00-R**	**11/7/00**
Study of the Optical Parameters of the 40m LIGO Prototype		
Lisa Goggin, Alan Weinstein		

Distribution of this draft:

This is an internal working note
Of the LIGO Project

California Institute of Technology
LIGO Project – MS 51-33
Pasadena, CA 91125
Phone (626)395-2129
Fax (626)304-9834
E-mail: info@ligo.caltech.edu

Massachusetts Institute of Technology
LIGO Project – MS 20B-145
Cambridge, MA 01239
Phone (617)253-4824
Fax (617)253-7014
E-mail: info@ligo.mit.edu

WWW: http://www.ligo.caltech.edu

Study of the Optical Parameters of the 40m LIGO Prototype

Lisa Maria Goggin
Mentor: Professor Alan Weinstein
September 2000

Abstract:

The objective of my project was to model the interferometer optics of the 40m LIGO prototype with regard to cavity lengths, mirror radii of curvature and beam spot sizes and beam radii of curvature in both the cases of flat and curved input test mass. This study also includes the design of a 12m mode-cleaner and evaluation of its performance on suppression of higher order modes. We present the optical design of mode-matching telescopes, which are necessary to match the beams from the resonant cavities of the prestablized laser, mode cleaner and interferometer.

1. Introduction

LIGO, the Laser Interferometer Gravitational-Wave Observatory is a project dedicated to the detection of gravitational waves and the harnessing of these waves for scientific research. Gravitational waves, which are emitted by accelerated masses, were first predicted by Einstein in 1916 in his general theory of relativity. They have not yet been observed although their presence has been indirectly verified.

LIGO consists of two widely separated sites, one at Hanford, Washington, the other in Livingston, Louisiana. These sites house power recycled Michelson interferometers with Fabry-Perot arms 4 kilometers in length. These sites have been constructed and the detectors are currently being installed. The LIGO I data run is to commence in 2003.

Even before LIGO1 comes online, plans for modifications and improvements to the current set-up are already well under way. The advanced LIGO II configuration will be installed in 2005. Before these changes can be implemented they have to be tested, and this is the purpose of the 40m lab on campus. This lab contains a 40m LIGO prototype, that is a power recycled Michelson interferometer with Fabry-Perot arms 40m in length. This is currently being upgraded to become as LIGO 1 like as possible. The features of the upgrade that motivated my project are the replacement of the green laser by an infrared laser and the adoption of the LIGO 1 mode cleaner design.

For my SURF I worked at the 40m lab, my project being concerned with modeling the input optics and interferometer and measuring the properties of the beam throughout using *Matlab*. Section 2 of this report discusses relevant properties of Gaussian beam optics and resonators. The components of the input optics and interferometer that my project was concerned with are introduced in section 3. Section 4 presents a more in-depth discussion of the methods that led to our results.

2.Theory:

2.1 Gaussian Beams:

The scalar wave equation for electromagnetic fields in free space is given by

$$\tilde{N}^2 E + k^2 E = 0 \tag{2.1.1}$$

where k = 2πλ, where λ is the wavelength of light in the medium.
For light traveling in the z direction

$$E = Y(x, y, z)\, e^{-ikz} \tag{2.1.2}$$

where the function $Y(x, y, z)$ represents a spatial modulation of the plane wave.
Substitution of (2.1.2) into (2.1.1), taking account of the paraxial approximation:

$$2ik\frac{\partial Y}{\partial z} >> \frac{\partial^2 Y}{\partial z^2} \tag{2.1.3}$$

i.e. that the longitudinal variation in the modulation function changes very slowly, gives

$$\frac{\partial^2 Y}{\partial x^2} + \frac{\partial^2 Y}{\partial y^2} - 2ik\frac{\partial Y}{\partial z} = 0 \tag{2.1.4}$$

This is the paraxial approximation of the wave equation.
A trial solution of (2.1.4) is

$$Y = g\left(\frac{x}{w}\right) h\left(\frac{y}{w}\right) \exp\left(-iB\left(p + \frac{k}{2q}(x^2 + y^2)\right)\right) \tag{2.1.5}$$

where g is a function of x and z and h is a function of y and z. ω(z) is a measure of the decrease of the field amplitude with distance from the axis, and p(z) is a complex phase shift. q(z) is a complex beam parameter, which describes the Gaussian variation in the beam intensity with distance from the optic axis as well as the curvature of the phase front.

Insertion of (2.1.5) into (2.1.4) yields a differential equation of a Hermite polynomial

$$\frac{d^2 H_m}{dx^2} - 2x\frac{dH_m}{dx} - 2mH_m = 0 \qquad (2.1.6)$$

which is satisfied if

$$g_h = H_m\left(\sqrt{2}\,\frac{x}{w}\right) H_n\left(\sqrt{2}\,\frac{y}{w}\right) \qquad (2.1.7)$$

Thus the intensity pattern in the cross section of such a beam is a product of a Hermite and a Gaussian function. The primary E and H field components in these beams are polarized transverse to the direction of propagation and hence these waves are referred to as TEM_{mn} optical waves, where m and n are integers known as transverse mode numbers. The most important solution for the paraxial equation however is that with a purely Gaussian intensity profile, the TEM_{00} mode. This is the only mode that is spatially coherent.

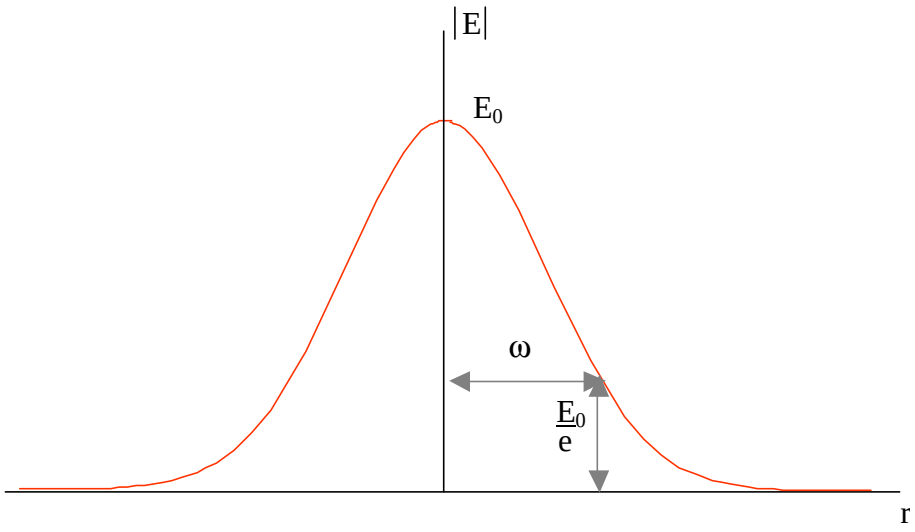

Fig. 2.1.1. Amplitude distribution of a Gaussian beam

2.2 Physical Properties of Gaussian Beams

The parameter ω is referred to as the beam radius or spot size. It is the distance normal to the direction of propagation at which the amplitude is 1/e times that on the axis. A Gaussian beam propagating through a homogeneous medium will have one unique minimum value of beam radius, ω_0 at a particular position, the beam waist.

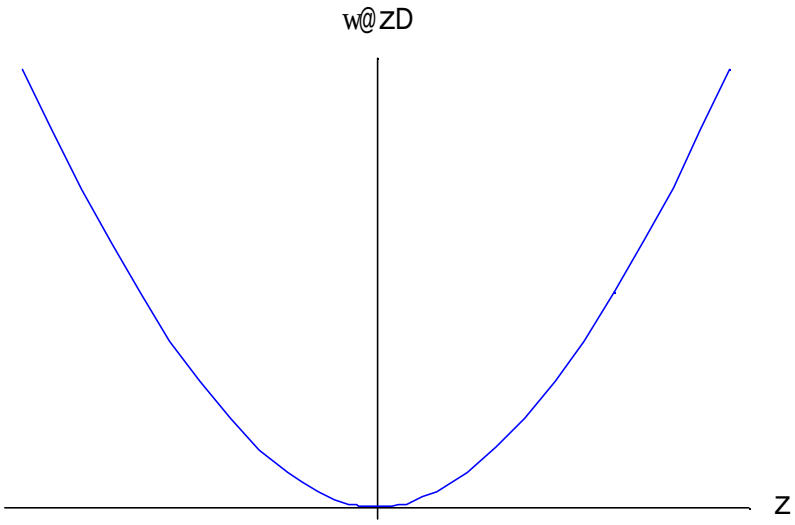

Fig. 2.2.1. Beam Radius versus Distance from Waist

The distance that the beam travels on the optic axis at either side of the waist before the beam radius increases by $\sqrt{2}$, or equivalently before the area doubles, is called the Rayleigh range, z_R. This marks the approximate dividing line between the 'near field' or Fresnel and the 'far field' or Fraunhofer regions for a beam propagating out from a Gaussian waist. The radius of curvature, R, of the wavefront is planar at the waist. As the beam propagates outward the wavefront gradually becomes curved and the radius of curvature rapidly drops to finite values. For distances well beyond the Rayleigh range the radius of curvature increases again as R(z)~z. The radius of curvature is taken to be positive if the wavefront is convex as viewed from z = ¥.

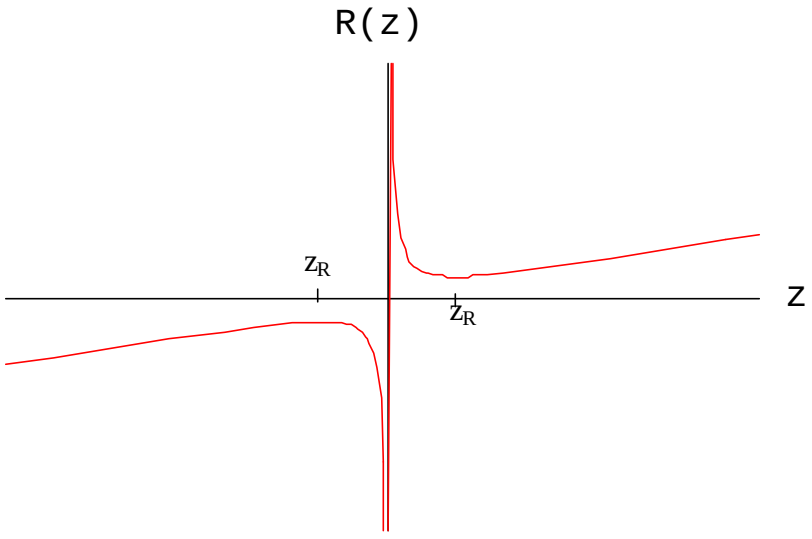

Fig. 2.2.2 Radius of Curvature of Wavefront versus Distance from Waist

The far-field beam angle, that is, the angle that the gaussian beam spreads at $z>>z_R$, is defined by the width corresponding to the 1/e point of the amplitude;

$$2\,\theta_{\frac{1}{e}} = \frac{2\,\lambda}{\pi\, w_0} \tag{2.2.1}$$

The beam divergence is the half angular spread

$$\theta_{\frac{1}{e}} = \frac{\lambda}{\pi\, w_0} \tag{2.2.2}$$

Both ω and R can be expressed in terms of z_R and z

$$w(z) = w_0 \sqrt{1 + \left(\frac{z}{z_R}\right)^2} \tag{2.2.3}$$

$$R(z) = z\left(1 + \left(\frac{z_R}{z}\right)^2\right) \tag{2.2.4}$$

The complex beam parameter q is defined in terms of R and ω

$$\frac{1}{q} = \frac{1}{R} - i\,\frac{\lambda}{\pi\, w^2} \tag{2.2.5}$$

hence, at the waist, q is purely imaginary

$$q_0 = -i\,\frac{\pi\, w_0^2}{\lambda} \tag{2.2.6}$$

and a distance z away from the waist

$$q = q_0 + z \tag{2.2.7}$$

The real part of the complex phase shift p, is known as the Guoy phase shift *h*,

$$\eta(z) = \tan^{-1}\left(\frac{z}{z_R}\right) \tag{2.2.8}$$

This has the effect of giving the lowest order mode a phase shift of 180^0 on passing through the waist, with most of this occurring within one or two Rayleigh ranges on either side of the waist. In physical terms this means that the phase velocity and the spacing between wavefronts are slightly larger than for an ideal plane wave. Higher order modes have larger Guoy phase shifts in passing through the waist region.

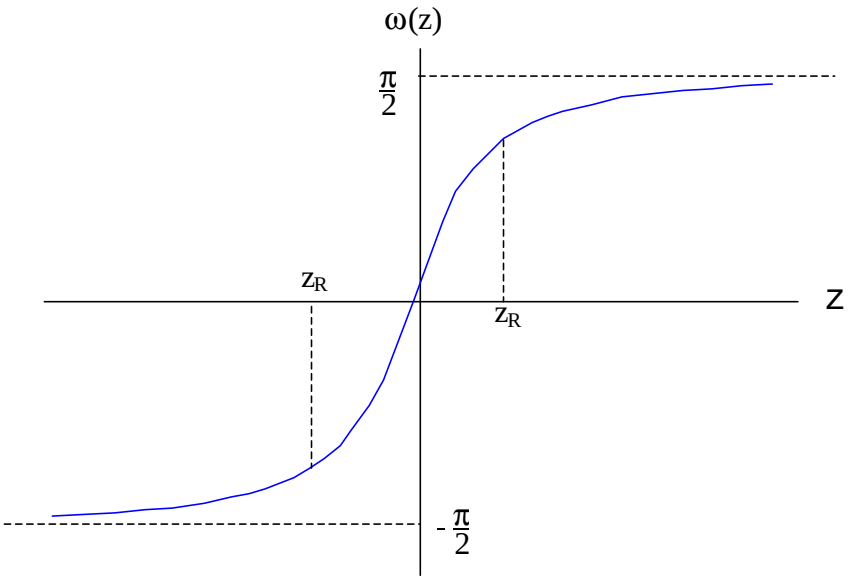

Fig. 2.2.3. Guoy phase shift through the waist region of a Gaussian beam

2.3 Optical Resonators:

It two curved mirrors, of radius of curvature R_1 and R_2, are placed anywhere in the path of a Gaussian beam, and if the radius of curvature of the wavefront exactly matches that of the mirrors, then an optical resonator is formed. The mirrors, a distance L apart, produce a standing wave, reflecting the beam back on itself with exactly reversed radius of curvature and direction. This is depicted in Fig. 2.3.1

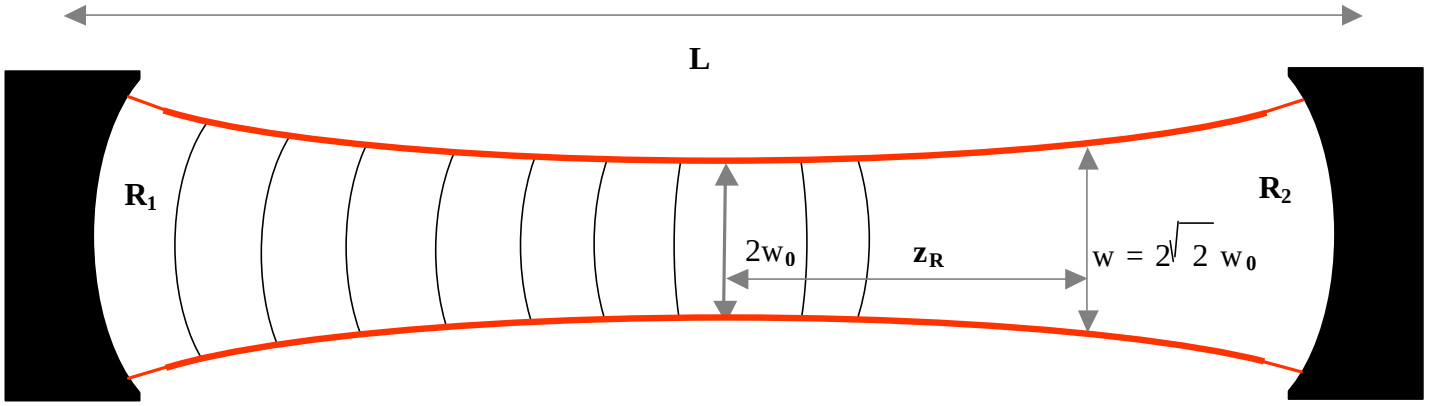

Fig. 2.3.1. Gaussian beam resonant cavity

The optical resonator can support both the lowest order Gaussian mode and the higher order Hermite-Gaussian modes as resonant modes of the cavity. These mirrors define a unique Rayleigh range for the Gaussian beam

$$z_R^2 = \frac{L^2 (L - R_1)(L - R_2)(R_1 + R_2 - L)}{R_1 R_2 (R_1 + R_2 - 2L)} \tag{2.3.1}$$

The distances of the mirrors R_1 and R_2 from the waist respectively are;

$$z_1 = \frac{L - R_2}{2L - R_1 - R_2}, \qquad z_2 = \frac{L - R_1}{2L - R_1 - R_2} \tag{2.3.2}$$

We can define a pair of 'resonator g-parameters' for each mirror.

$$g_1 = 1 - \frac{L}{R_1}, \qquad g_2 = 1 - \frac{L}{R_2} \tag{2.3.3}$$

The product of the g-factors is a measure of the stability of the cavity. The stability range is $0 \leq g_1 g_2 \leq 1$, as otherwise real and finite solutions for the gaussian beam parameters and spot sizes cannot exist. As the g-factor decreases below 1 the Guoy phase difference of higher order modes gets larger and only one mode resonates in the cavity. The total Guoy phase shift along the resonator length is given in terms of the g-parameters;

$$\eta(z_2) - \eta(z_1) = \cos^{-1} \cdot \sqrt{g_1 g_2} \tag{2.3.4}$$

The transmittance, T, of light from the cavity is given by

$$T = \left| \frac{t_1 t_2 e^{i\phi}}{1 - r_1 r_2 e^{2i\phi}} \right|^2 \tag{2.3.5}$$

where t_1 and t_2 are the coefficients of transmission, and r_1 and r_2 are the coefficients of reflection of mirrors 1 and 2 of the cavity, and ϕ is the phase shift.

2.4 Beam Propagation Through a Lens

A thin lens has the effect of changing the radius of curvature of a beam leaving the transverse field distribution of the mode unchanged. An ideal thin lens of focal length f transforms an incoming beam of radius of curvature R_1 to that of R_2 according to the following equation

$$\frac{1}{R_2} = \frac{1}{R_1} - \frac{1}{f} \qquad (2.4.1)$$

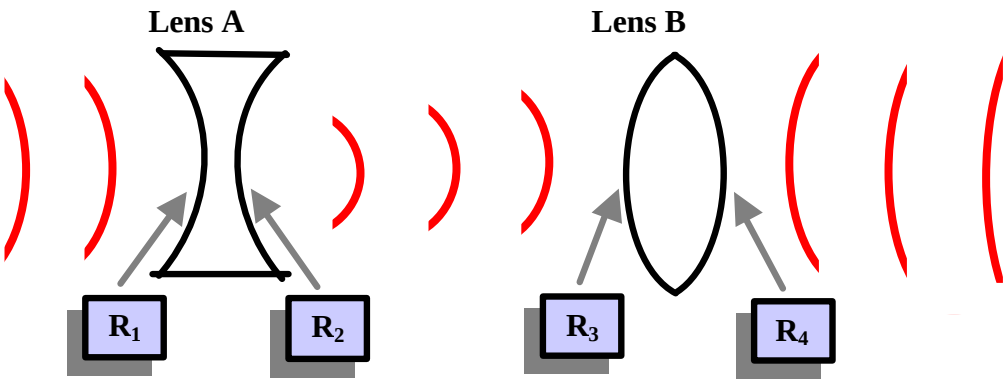

Fig. 2.4.1. Transformation of radius of curvature of beam as it passes through diverging and converging lens

The spot size of the beam is the exactly the same immediately to the left and to the right of such a lens and so the corresponding beam parameters are related by

$$\frac{1}{q_2} = \frac{1}{q_1} - \frac{1}{f} \qquad (2.4.2)$$

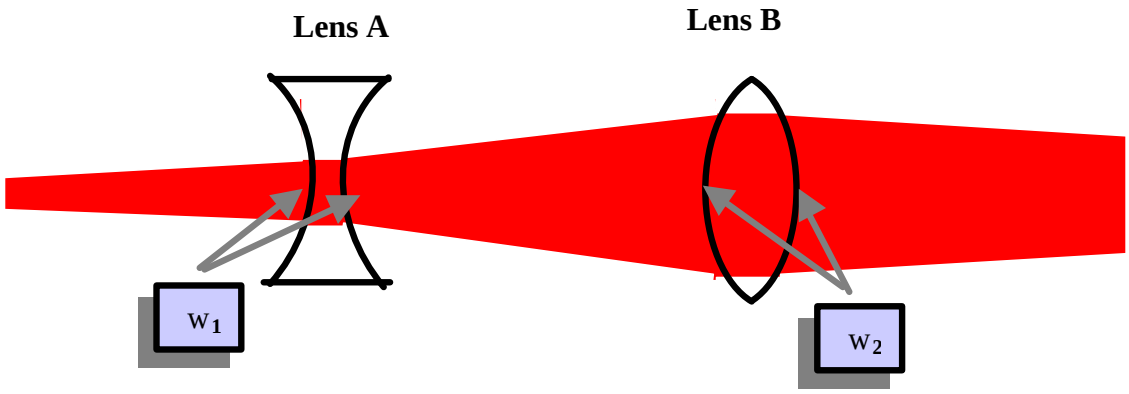

Fig. 2.4.2. Variation in beam radius in passing through diverging and converging lenses

2.5 Mode Mismatch

When the beam waist is axially translated, or of different size to that desired, the beam is said to be mismatched. The mismatch, m is defined as follows;

$$m = \sqrt{e^2 + b^2} \qquad (2.5.1)$$

where

$$e = \frac{w_{desired} - w_{actual}}{w_{actual}}, \qquad b = \frac{z_{desired} - z_{actual}}{2 z_R}$$

The square of the mode mismatch, m^2, is approximately the amount of beam power lost to the desired mode

3 Optical Configuration of the Caltech 40 meter Prototype Interferometer

3.1 The 40m Laboratory:

Fig. 3.1.1 gives a schematic overview of the optical configuration of the 40m interferometer. The beam of light travels from the laser on the left of the diagram through the pre-stabilized laser, (PSL), and on to the first mode matching telescope, (MMT1). From there the beam enters vacuum and into the mode cleaner resonant cavity, (MC) and on to the second mode matching telescope, (MMT 2). These make up the input optics. The beam then propagates on towards the interferometer. The beam encounters the recycling mirror, (RM) and then at the beam splitter (BS), is divided equally between the two arms of the interferometer.

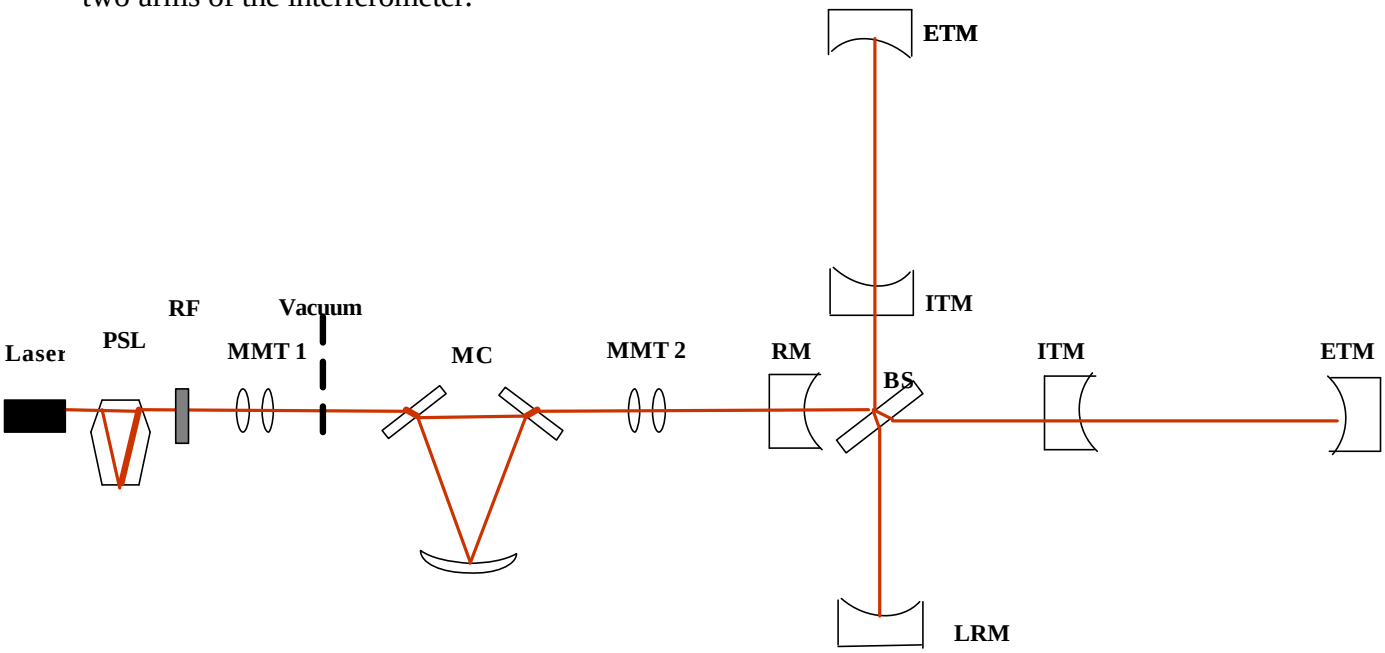

Fig 3.1.1 Schematic overview of the optics of the 40m LIGO prototype

3.2 The 40m Interferometer

When the laser light from the input optics (to be described below) reaches the beam splitter, half of the light goes to the inline arm and the other half to the perpendicular arm. The test masses each have one face highly polished and coated to form a mirror. The two curved mirrors along each arm form a Fabry-Perot cavity, and so the beam circulates many times. The end test mass has a much lower transmissivity and so the light exits the cavity through the input test mass and back to the beam splitter where the two beams are recombined. The majority of the light travels to the recycling mirror, where it is returned to the interferometer, coherently, to be reused; and the remainder is directed towards the photodiode at the 'dark' port. The highly reflecting recycling mirror forms one side of this over coupled resonant cavity and so the light is returned towards the beam splitter.

3.3 Mode Cleaner:

A mode cleaner is a device that provides frequency and spatial stabilization of the laser light before it reaches the interferometer. It does this by transmitting the TEM_{00} mode of the laser light and reflecting the higher order modes. The mode cleaner presently at the 40m lab consists of two curved mirrors a distance of 1m apart. The upgraded mode cleaner is to be more 'LIGO-like', consisting of two plane mirrors and one curved mirror in a triangular configuration, approximately 12m in length. This configuration can be treated just as the linear resonator discussed earlier. The plane mirrors are purely for directing the beam, they do not affect its radius of curvature or spot size and so the curved mirror acts as both ends of the resonator. The length of this cavity is the distance the beam travels in one complete round of the cavity. As the 'end mirrors' are identical the waist lies in the middle of the cavity, that is, midway between the two plane mirrors. The triangular configuration of the mode cleaner ensures that the reflected light is directed away from the path of the incoming beam.

3.4 Mode-Matching Telescopes

In the set-up we have three resonant cavities: the pre stabilized laser, the mode cleaner and the interferometer, (itself a set of four coupled cavities). Each of these defines a unique beam with a particular beam waist and radius of curvature. As the laser beam circulates through each of these it is necessary to have a device that transforms the beam so that it will resonate in each cavity. This is achieved using mode-matching telescopes. At the 40m, these consist of two lenses whose curvature and separation control the radius of curvature and spot size of emerging beam. (The LIGO mode matching telescopes consist of three suspended mirrors.) Using a given separation of the lenses and equations (2.2.3), (2.2.4) and (2.3.6) it is possible to solve exactly for the focal lengths. These custom focal-length lenses are, however, quite expensive to make. A much more cost effective solution is to use 'off the shelf' lenses, that is, lenses that are freely available for particular focal lengths. Therefore, for a given pair of lenses, we vary the lens separation until we find the position of minimum mode mismatch.

3.5 Mode Mismatch

Solving our mode matching telescope problem in this manner may not always lead to exact solutions. If the focal lengths chosen are slightly larger or smaller than those required for the resulting separation, then the radius of curvature and spot size of the beam beyond the telescope are a little different to what we expected. As a result, the beam is not mode-matched properly into the cavity and this results in some higher order modes. The 'best-fit' lenses are those that minimize the mode-mismatch, defined in equation (2.5.1).

4 Results:

4.1 Interferometer

In our study we considered both the cases of a symmetric and half-symmetric interferometer. (In a symmetric interferometer the input test mass (ITM) and the end test mass (ETM) are identical. A half-symmetric interferometer has a plane input test mass and a curved end test mass.) As discussed in section 2.3, in order for the cavity to be resonant and to eliminate mode mismatch, the radius of curvature of the mirror has to exactly match that of the beam at the point at which the mirror is to be placed. Using equations (2.2.3) through (2.2.7) and the specified distances between optics, the spot size and radius of curvature of the beam, and hence the radius of curvature of the mirrors were found. Fig 4.1.1 displays our results.

(a)

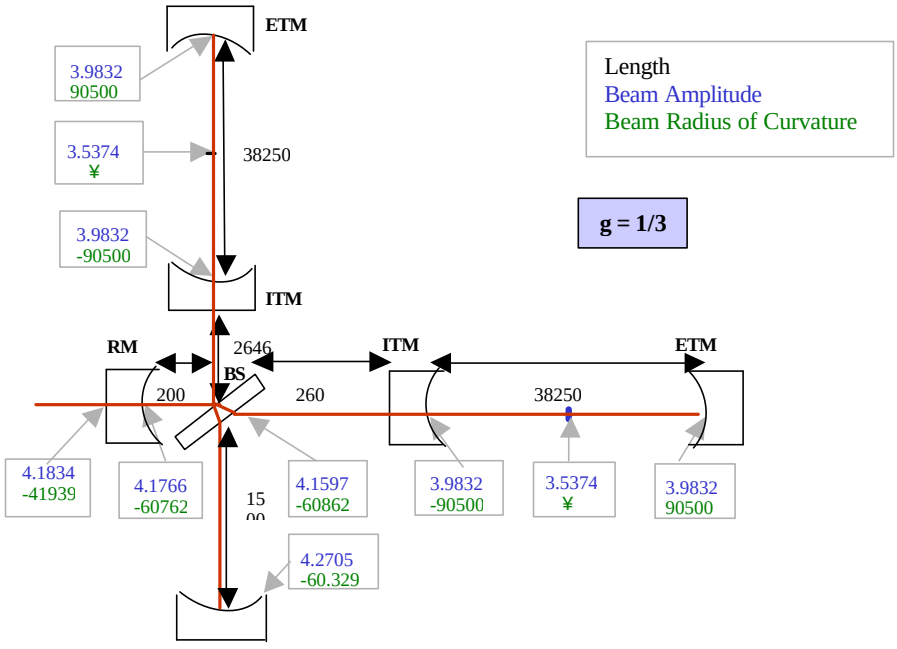

(b)

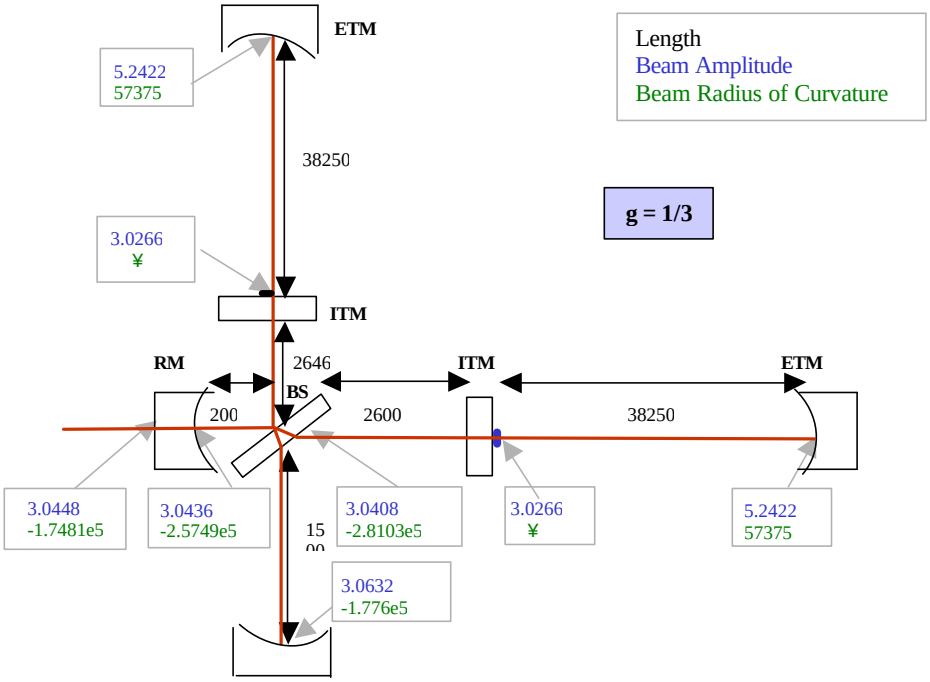

Fig. 4.1.1. Beam parameters in (a) symmetric and (b) half-symmetric interferometer

4.2 Mode Cleaner

In modeling the mode cleaner for the 40m lab upgrade we used the LIGO 1 design*. This consists of two plane mirrors and one curved mirror. These are housed in a 12m vacuum pipe, with the two flat mirrors at one end and the curved mirror at the other. Light from the laser reaches the first flat mirror, FM1, where the majority of it is reflected. The rest of the light is transmitted and travels towards the second flat mirror, FM2, encountering the beam waist midway between FM1 and FM2. Here, a small amount of the light is transmitted and the rest is reflected towards the curved mirror. As in the case of the interferometer, the radius of curvature of the beam at the point at which the curved mirror is to be placed determines its radius of curvature. The spot size is largest at the curved mirror. On being reflected the wavefront radius of curvature is exactly reversed and the spot size begins to decrease. The beam returns to FM1, where again, a small proportion is transmitted and the rest is reflected.

The portion of the beam consisting of the TEM00 mode resonates in the cavity, and so tends to be transmitted. That transmitted at FM1 is exactly out of phase with the incoming reflected light, and so they interfere destructively. The TEM00 light reflected at FM1 is exactly in phase with the light entering the cavity. These interfere constructively, causing the light circulating in the cavity to build up. The TEM00 light transmitted at FM2 travels on towards the interferometer.

(* see References)

Because of their larger Guoy phase shift, higher order modes do not resonate in the cavity and so, do not interfere constructively with the incoming light. For this reason higher order modes do not build up in the cavity. Similarly, higher order modes do not interfere destructively with the incoming reflected light and so are not transmitted. By design, no light is transmitted at the curved mirror.

Using equation (2.2.3) through (2.2.4), the beam was traced throughout the cavity. Fig 4.2.1 displays our results for the radius of curvature and spot size of the beam at the flat and curved mirrors.

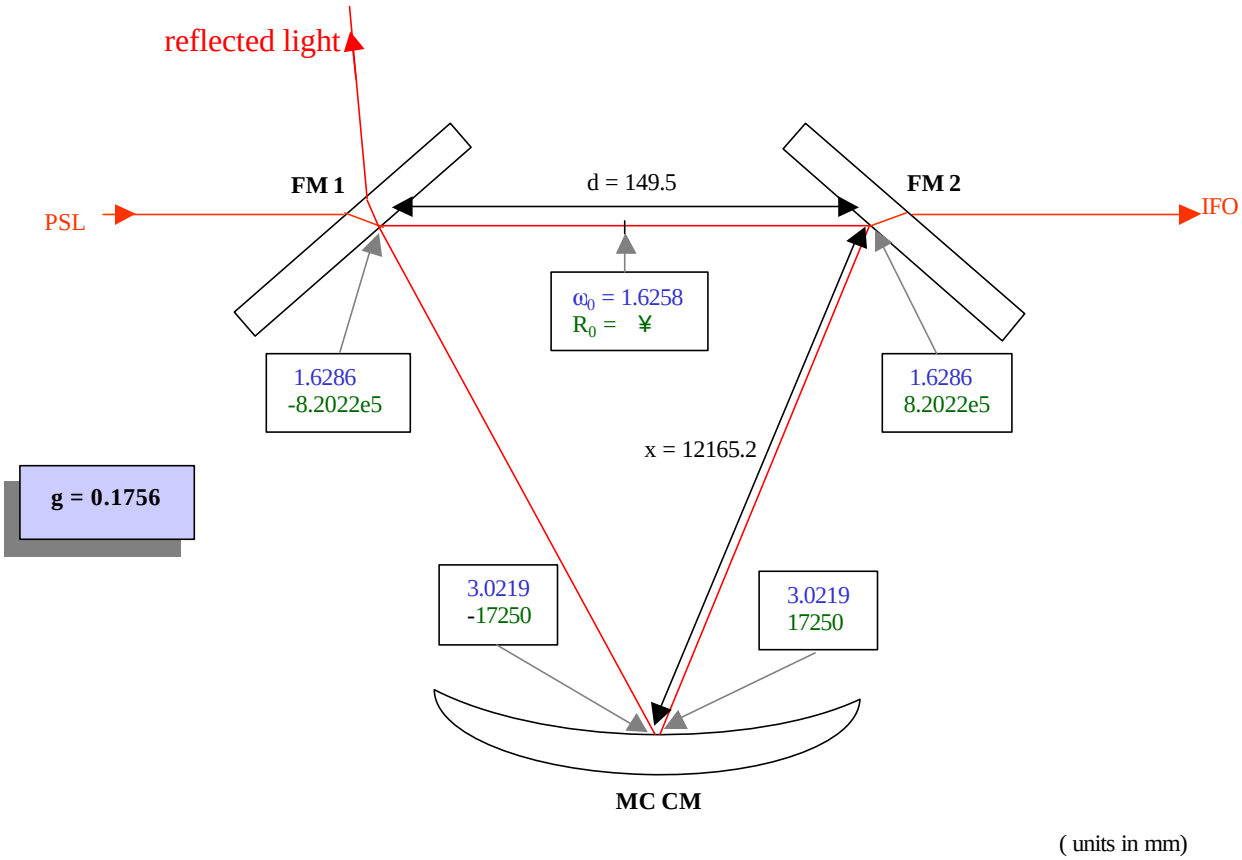

Fig. 4.2.1. Beam parameters for mode cleaner

The performance of the mode cleaner is assessed in Fig 4.2.2. For given values of r_1, r_2, t_1 and t_2, equation (2.3.5) was used to calculate the transmittance of the lowest order and higher order modes.

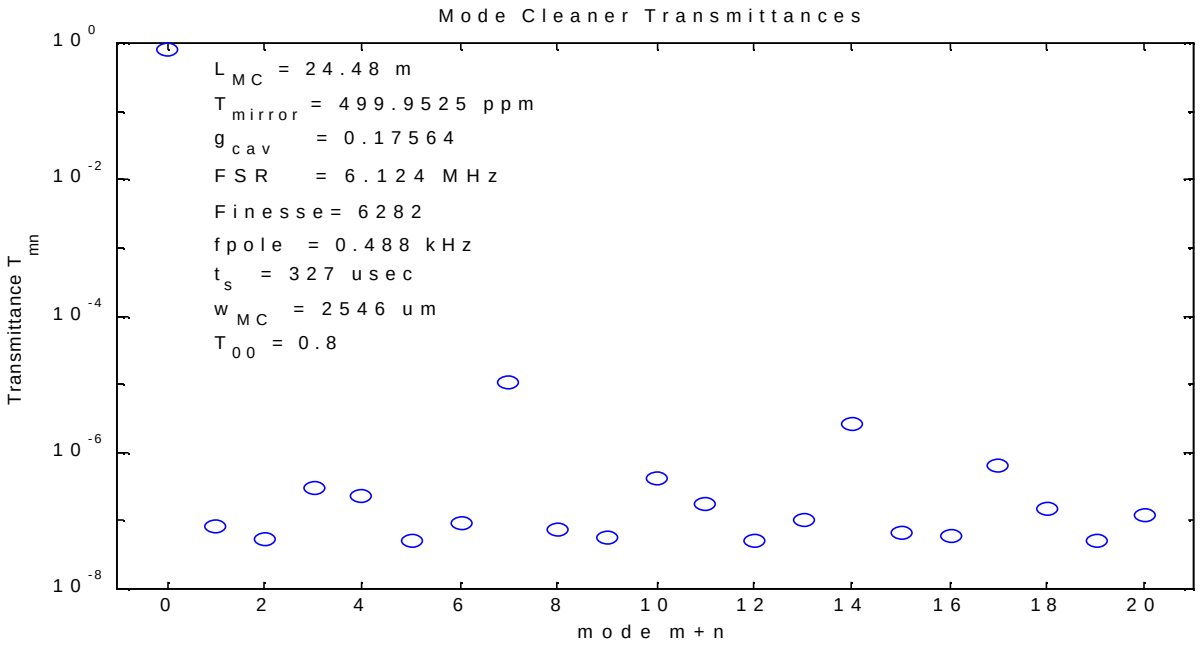

Fig. 4.2.2. Graph of transmittance versus mode number for the mode cleaner resonant cavity

4.3 Mode-Matching Telescopes

The two lenses of the mode-matching telescope are mounted on a motorized rail to adjust the distance. The rail is graduated so the distance between the lenses can be accurately measured. In designing these mode-matching telescopes, we first made the assumption that the distance to the waist of the intermediate beam formed between the two lenses was much greater than the Rayleigh length.

i.e. $$\frac{z}{z_R} >> 1 \qquad (4.3.1)$$

and so equation (2.2.3) simplifies to

$$w(z) = w_0 \left| \frac{z}{z_R} \right| \qquad (4.3.2)$$

This is valid as the beam divergence at z (equation (2.2.2)) is very small.

The initial separation was chosen to 15cm, as this gave plenty room for adjustment on either side of the lenses. Using our knowledge of the parameters of the resonant cavity on either side of the telescope, we found the radius of curvature of the beam entering the telescope and what the radius of curvature the beam should have leaving the telescope. This also told us the spot size of the beam inside the telescope, as the spot size is the same (immediately) on either side of a thin lens. Thus, we found the radius of curvature

of the intermediate beam formed between the lenses, using equations (4.3.2) and (2.2.4). We can then found the focal lengths using equation (2.4.1).
The Melles-Griot catalogue lists available focal lengths for fused silica of refractive index corresponding to a wavelength of 514nm. Since we were working with a wavelength of 1064nm, the following equation enables us to translate between these.

$$f_1 (n_1 - 1) = f_2 (n_2 - 1) \qquad (4.3.3)$$

where f_i and n_i are the focal lengths and refractive indices corresponding to wavelengths λ_i.

Comparing the focal lengths of the available and required lenses, a suitable pair was selected. Their separation was varied until the minimum mode mismatch was found. Fig. 4.3.1 displays the chosen focal and resulting separations of the lenses. A positive value of f indicates a converging lens, while a negative value denotes a diverging lens.

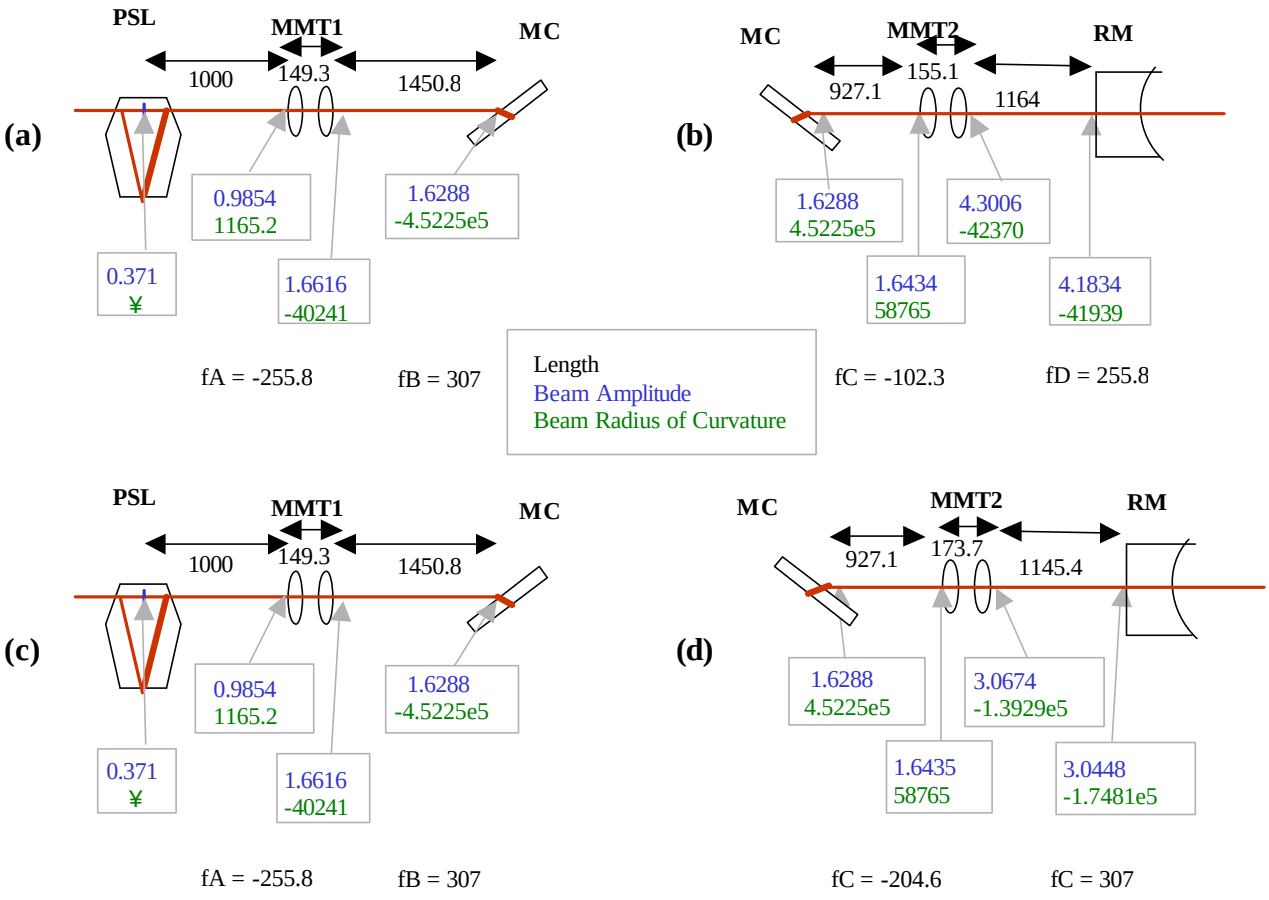

Fig. 4.3.1. Beam and lens parameters for (a) mode matching telescope 1 and (b) mode matching telescope 2 for the symmetric interferometer. (c) mode matching telescope 1 and (d) mode matching telescope 2 for the half symmetric interferometer.

4.4 Mode Mismatch

Using these focal lengths and separations the actual beam emerging from the telescope was traced to its waist in the cavity. Neither the position nor the amplitude was what we initially expected for that particular cavity, and so the beam was mismatched.

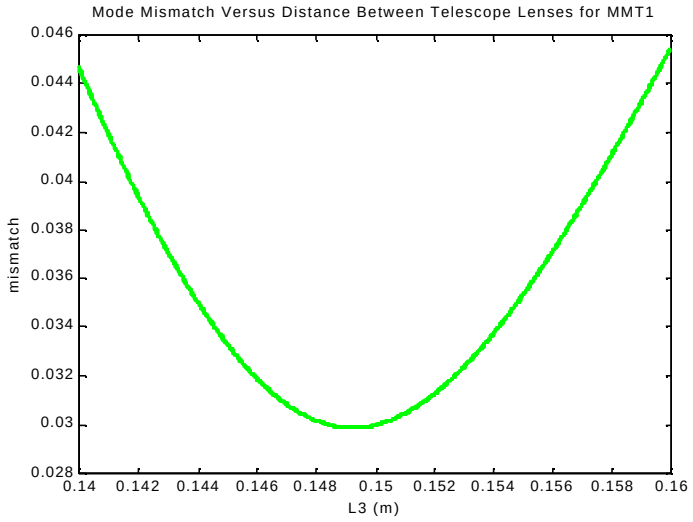

mode mismatch = 0.03
distance between lenses =149.25mm

fA(λ=1064) = -255.8 mm
fB(λ=1064) = 307 mm

(a)

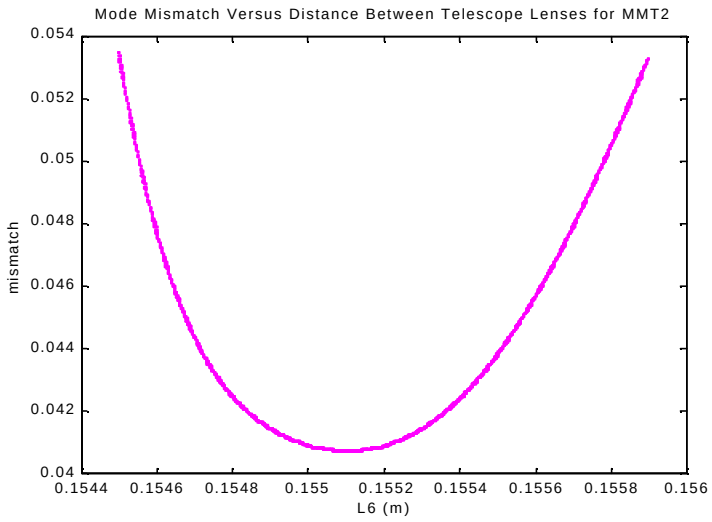

mode mismatch = 0.0407
distance between lenses =155.1mm

fC(λ=1064) = -102.3 mm
fD(λ=1064) = 255.8 mm

(b)

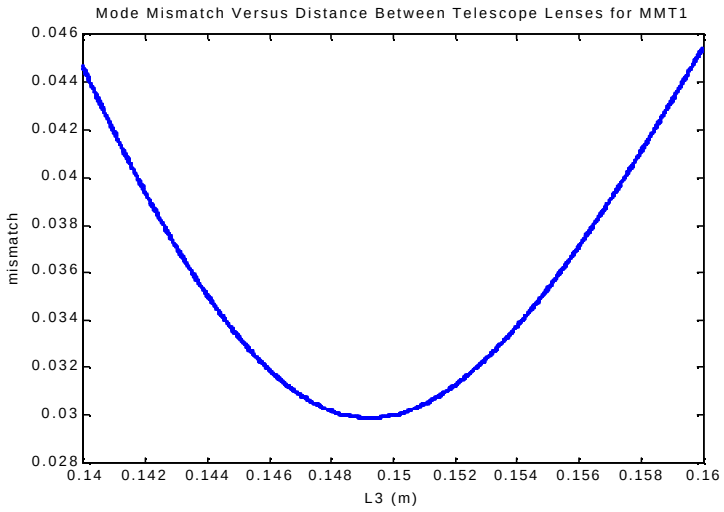

mode mismatch = 0.03
distance between lenses =149.25mm

fA(λ=1064) = -255.8 mm
fB(λ=1064) = 307 mm

(c)

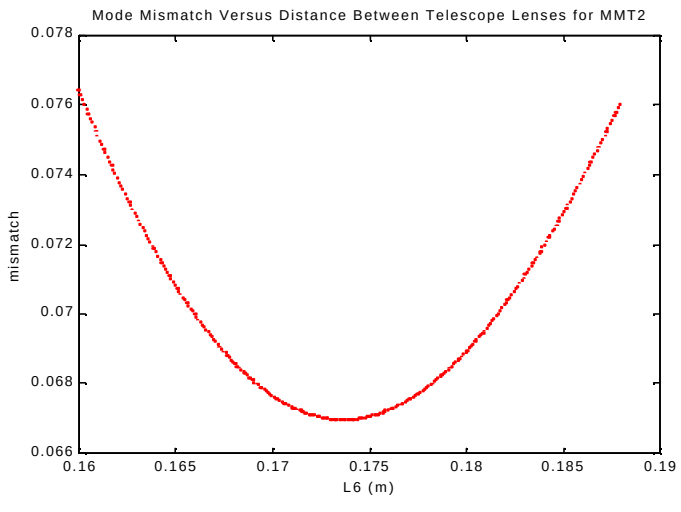

mode mismatch = 0.0669
distance between lenses =173.68mm

fC(λ=1064) = -204.6 mm
fD(λ=1064) = 307 mm

(d)

Fig. 4.4.1. (a), (b), Modes mismatch versus lens separation for telescopes 1 and 2 respectively, (symmetric interferometer). (c), (d) mode mismatch versus lens separation for telescopes 1 and 2, (half symmetric interferometer).

To find the position of minimum mode mismatch the separation of the lenses was varied over a short interval and the mode mismatched was calculated for each point. As can be seen in the graphs of Fig 4.4.1 the mode mismatch decreased to a minimum at a particular separation before increasing again. The values of the mismatch, focal lengths of the lenses and lens separation is listed for each case.

5 Discussion

Both the symmetric and half-symmetric interferometers were studied and from the results both seem feasible. In each, the radius of the beam is smaller than the size of the optics (3 inches). However the half-symmetric interferometer was chosen the beam waist is clearly visible at the input test mass. The radius of curvature and spot size of the beam were specified at all important points throughout the interferometer. Using this information the radius of curvature of the mirrors was established.

The radius of curvature of the end mirror in the mode cleaner is small compared to the length of the cavity and thus the value of the g-factor for the cavity is small. As a result the Guoy phase shift of the higher order modes is large and so only the TEM_{00} mode will resonate. Thus the beam leaving the mode cleaner will be highly stabilized. As can be seen from Fig. 4.2.2, this design in mode cleaner is successful in suppressing the higher order modes. 80% of the TEM_{00} mode is transmitted whereas the next highest transmission (of a higher order mode) is approximately 0.01%.

As can be seen from the graphs in Fig. 4.3.1 the mode mismatch is very small and so it appears that using off the shelf lenses in the telescopes will not create a problem. Symmetric biconcave and biconvex lenses were chosen over plano-concave/convex as this design minimized spherical aberration and cancelled out coma and distortion.

6 Acknowledgments

I wish to thank my mentor Alan Weinstein for his help both during the summer and in writing this paper. I also want to thank Dennis Ugolini and Steve Vass for their help in the lab. Finally thanks to Ken Libbrecht and the SURF program for giving me the opportunity to work on the LIGO project.

7 References

- Siegman; '*Lasers*'
- Kogelnik & Li; 'Laser Beams and Resonators', *Appl. Opt.*, vol. 5, pp. 1550-67, Oct 1966
- Anderson; 'Alignment of Resonant Optical Cavities', *Appl. Opt.*, vol. 23, pp 2944-49, Sep. 1984
- Boyd; 'Intuitive Explanation of the Phase Anomaly of focused Light Beams', *j. Opt. Soc. Am.*, vol 70, pp 877-80, Jul. 1980
- Abramovici et al; 'LIGO: The Laser interferometer Gravitational-Wave Observatory', *Science*, vol. 256, pp 325-33, 17 Apr. 1992
- * R. Adhikari et al; 'Input Optics Final Design Document, Rev. 01', LIGO T-980009, 1998
- Melles-Griot; *Optics Guide 5*

Appendix 1

Abbreviations:

PSL	pre stabilized laser
MMT	mode matching telescope
MC	mode cleaner
FM1	flat mirror 1
FM2	flat mirror 2
MC CM	mode cleaner curved mirror
RM	recycling mirror
BS	beam splitter
IMT	input test mass
ETM	end test mass
LRM	light recycling mirror

Appendix 2
Constants:

Quantity	Symbol	Value	Unit
wavelength of Nd:Yag laser	λ	1.064	mm
refractive index of fused silica	nfs(λ=1.064)	1.44963	
refractive index of fused silica	nfs(λ=0.514)	1.46008	
thickness of curved mirrors	d_cm	0.1	m
thickness of plane mirrors	d_pm	0.04	m

Appendix 3
Summary of Results:

1. Symmetric Arms:

1.1 Lengths:

(a) Interferometer:

Distance from	to	value / m
RM	BS	0.2
BS	LRM	1.5
BS	ITM (in-line)	2.6
ITM	ETM	38.25
BS	ITM (off-line)	2.646
ITM	ETM	38.25

(b) Mode Cleaner

Distance from	to	value / m
plane mirror 1	plane mirror 2	0.1495
plane mirror 1, 2	curved mirror	12.1652

(c) Mode Matching Telescope 1

Distance from	to	value / m
PSL	Lens A	1
Lens A	Lens B	0.1493
Lens B	MC	1.4508

(d) Mode Matching Telescope 2

Distance from	to	value / m
MC	Lens C	0.9271
Lens C	Lens D	0.1551
Lens D	RM	1.164

1.2 Cavity Details:

(a) Interferometer:

Quantity	Symbol	Value	Unit
cavity g-factor	g	0.3333	-
cavity length	L	38.25	m
distance of waist from ITM		19.125	m
waist size	w0	3.5374	mm

Beam Parameters

Item	w/mm	R/m
RM (left)	4.1834	-41.939
RM (right)	4.1766	-60.762
BS	4.1597	-60.862
LRM	4.2705	-60.329
ITM (inline, interior)	3.9832	-90.5
ETM (inline, interior)	3.9832	90.5
ITM (offline, interior)	3.9832	-90.5
ETM (offline, interior)	3.9832	90.5

(b) Mode Cleaner

Quantity	Symbol	Value	Unit
cavity g-factor	g	0.1756	-
cavity length	L	24.48	m
flat mirror coefficient of transmittance	t1, t2	0.02236	
flat mirror coefficient of reflectance	r1, r2	0.9997	
distance of waist from plane mirror	d/2	74.75	mm
waist size	w0	1.6258	mm

Beam Parameters

Item	w/mm	R/m
plane mirror 1 (exterior)	1.6288	-452.25
plane mirror 1 (interior)	1.6286	-820.22
curved mirror	3.0219	17.250
plane mirror 2 (interior)	1.6286	820.22
plane mirror 2 (exterior)	1.6288	452.25

(c) Mode Matching Telescope 1

Quantity	Symbol	Value	Unit
lens A, focal length	fA	-255.8	mm
lens B, focal length	fB	307	mm

Beam Parameters

Item	w/mm	R/m
PSL	0.371	inf
lens A (left of)	0.9854	1.1652
lens A (right of)	0.9854	0.2098
lens B (left of)	1.6616	0.3094
lens B (right of)	1.6616	-40.241

(d) Mode Matching Telescope 2

Quantity	Symbol	Value	Unit
lens C, focal length	fC	-102.3	mm
lens D, focal length	fD	255.8	mm

Beam Parameters

Item	w/mm	R/m
lens C (left of)	1.6434	58.765
lens C (right of)	1.6434	0.1021
lens D (left of)	4.3006	0.2574
lens D (right of)	4.3006	-42.37

2 Half Symmetric Interferometer:

2.1 Lengths

(a) Interferometer:

distance from	to	value / m
RM	BS	0.2
BS	LRM	1.5
BS	ITM (in-line)	2.6
ITM	ETM	38.25
BS	ITM (off-line)	2.646
ITM	ETM	38.25

(b) Mode Cleaner

distance from	to	value / m
plane mirror 1	plane mirror 2	0.1495
plane mirror 1, 2	curved mirror	12.1652

(c) Mode Matching Telescope 1

distance from	to	value / m
PSL	Lens A	1
Lens A	Lens B	0.1493
Lens B	MC	1.4508

(d) Mode Matching Telescope 2

distance from	to	value / m
MC	Lens C	0.927
Lens C	Lens D	0.1737
Lens D	RM	1.1454

2.2 Cavity Details

(a) Interferometer:

Quantity	Symbol	Value	Unit
cavity g-factor	g	0.3333	-
cavity length	L	38.25	m
distance of waist from ITM	L/2	0	m
waist size	w0	3.0166	mm

Beam Parameters

Item	w/mm	R/m
RM (left)	3.0448	-174.81
RM (right)	3.0436	-257.49
BS(right)	3.0408	-281.03
LRM(interior)	3.0632	-177.6
ITM (inline, interior)	3.0266	inf
ETM (inline, interior)	5.2422	57.375
ITM (offline, interior)	3.0266	inf
ETM (offline, interior)	5.2422	57.375

(b) Mode Cleaner

Quantity	Symbol	Value	Unit
cavity g-factor	g	0.1756	-
cavity length	L	24.48	m
flat mirror coefficient of transmittance	t1, t2	0.02236	
flat mirror coefficient of reflectance	r1, r2	0.9997	
distance of waist from flat mirror	d/2	74.75	mm
waist size	w0	1.6258	mm

Beam Parameters

Item	w/mm	R/m
plane mirror 1 (exterior)	1.6288	-452.25
plane mirror 1 (interior)	1.6286	-820.22
curved mirror	3.0219	17.25
plane mirror 2 (interior)	1.6286	820.22
plane mirror 2 (exterior)	1.6288	452.25

(c) Mode Matching Telescope 1

Quantity	Symbol	Value	Unit
lens A, focal length	fA	-255.8	mm
lens B, focal length	fB	307	mm

Beam Parameters

Item	w/mm	R/m
PSL	0.371	inf
lens A (left of)	0.9854	1.1652
lens A (right of)	0.9854	0.2098
lens B (left of)	1.6616	0.3094
lens B (right of)	1.6616	-40.241

(d) Mode Matching Telescope 2

Quantity	Symbol	Value	Unit
lens C, focal length	fC	-204.6	mm
lens D, focal length	fD	307	mm

Beam Parameters

Item	w/mm	R/m
lens C (left of)	1.6434	58.765
lens C (right of)	1.6434	0.2039
lens D (left of)	3.0674	0.3063
lens D (right of)	3.0674	-139.29

Input Optics and Interferometer Parameters, (Symmetric Arms)

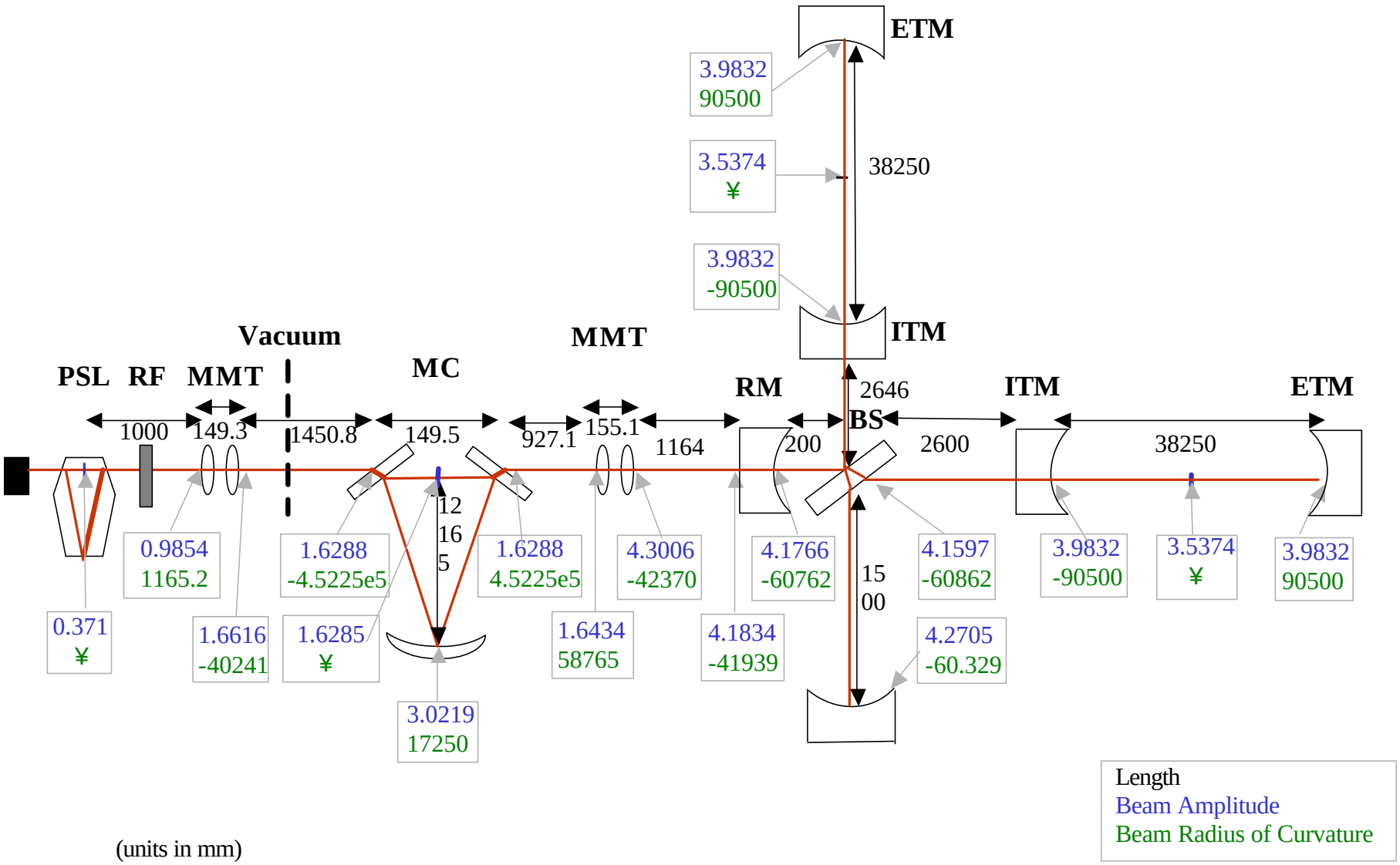

(units in mm)

Input Optics and Interferometer Parameters, (Half-Symmetric Arms)

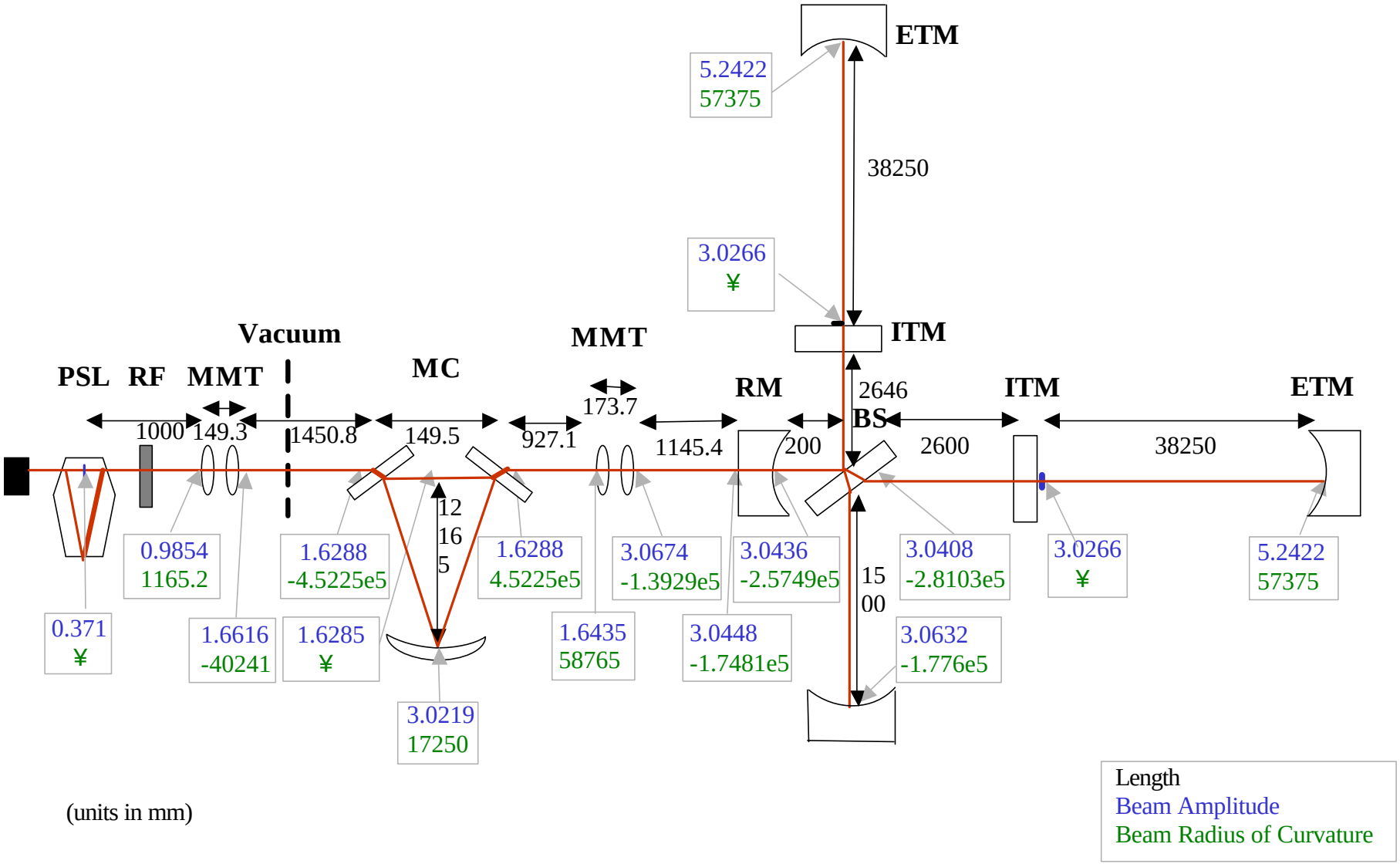

(units in mm)